A Theoretical Study on the Hydrolysis Process of the Antimetastatic Ruthenium(III) Complex NAMI-A

Jincan Chen,[†] Lanmei Chen,[†] Siyan Liao,[†] Kangcheng Zheng,*[,†] and Liangnian Ji*[,†,‡]

Department of Chemistry, Key Laboratory of Bioinorganic and Synthetic Chemistry of Ministry of Education, The Key Laboratory of Gene Engineering of Ministry of Education, State Key Laboratory of Optoelectronic Materials and Technologies, Sun Yat-Sen University, Guangzhou, 510275, China, and Department of Chemistry, Tongji University, Shanghai, 200092, China

Received: February 12, 2007; In Final Form: March 21, 2007

A hydrolysis process of the anticancer drug ImH[*trans*-Ru(III)Cl_4(DMSO)(Im)] (nicknamed NAMI-A; Im = imidazole, DMSO = dimethyl sulfoxide) has been studied by using density functional theory (DFT) method, and the aqueous solution effect has been considered and calculated by conductor-like polarizable calculation model (CPCM). The stationary points on the potential energy surfaces for the first and second hydrolysis steps (including two different paths) were fully optimized and characterized. The following was found: for the first hydrolysis process, the computed relative free energies $\Delta G°$ (aq) and rate constant (k) in aqueous solution are 23.2 kcal/mol and 6.11×10^{-5} s^{-1}, respectively, in satisfactory agreement with the experimental values; for the second hydrolysis step, some disagreement still exists, and thus more accurate solvent model needs to be designed and improved. On the basis of our present limited work, it can reasonably suggest that the hydrolysis process of NAMI-A perform mainly via the first hydrolysis step and then the path 1 of the second hydrolysis step. The theoretical results provide the structural properties as well as the detailed energy profiles for the mechanism of hydrolysis of NAMI-A, such results may assist in understanding the reaction mechanism of the anticancer drug with the biomolecular target.

I. Introduction

cis-[$PtCl_2(NH_3)_2$] (cisplatin) is one of the most widely utilized antitumor drugs in the world.[1,2] It is highly effective in treating a number of cancers, especially testicular and ovarian cancers, but this kind of drug has some side effects, such as severe renal toxicity, neurotoxicity, and emesis; thus, its applicability is still limited to a relatively narrow range of tumors.[3] These shortcomings, along with the fact that some tumors have natural resistance to cisplatin, have resulted in considerable researches focused on the development of more effective nonplatinum drugs that have less side effects and can be easily administered.[3] In the design of these new drugs, ruthenium complexes have raised a great interest for their potential use as therapeutic anticancer agents and lower systemic toxicity than platinum(II) compounds.[4−7]

Recently, several types of ruthenium(II) complexes with arene ligands[8,9] or heterocyclic bidentate ligands[10,11] have been proven to have a significant antitumor activity. However, the ruthenium-(III) complexes, such as Keppler-type complexes (HL)[*trans*-$RuCl_4L_2$], with a heterocyclic nitrogen ligand L, have shown promising results on colorectal autochthonous tumors.[5,7] *Mer*-[Ru(III)(terpy)Cl_3] (terpy = 2,2:6,2-terpyridine) exhibits an antitumor activity midway between those of cisplatin and carboplatin in the L1210 cell line.[12] The most promising antimetastatic agent, ImH[*trans*-$RuCl_4$(DMSO)(Im)] (nicknamed NAMI-A; Im = imidazole, DMSO = dimethyl sulfoxide), developed by Sava et al., is the first ruthenium anticancer complex that has entered clinical testing and recently has finished in the clinical trials of the first phase as an antimetastatic drug.[13] NAMI-A is pseudooctahedral with four equatorial chloride ligands, and DMSO and imidazole as axial ligands (Figure 1).[14] Preclinical pharmacological studies with NAMI-A showed a selective activity against lung metastases of murine tumors[14−16] and a relatively low toxicity in mice and dogs.[17−19]

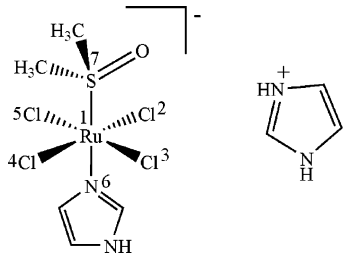

Figure 1. Chemical Structure of NAMI-A.

Although the mechanism of action of NAMI-A is not completely understood, it appears to be accepted that this drug can hydrolyze rapidly in vivo, forming a number of potentially active species.[20] Even though cisplatin is a square planar structure and NAMI-A is an octahedron structure as well as they have different types of ligands, NAMI-A has been shown to undergo similar substitution reactions of chloride by water to cisplatin,[20,21] and a degradation pathway has been proposed by Mestroni and Sava et al.[14,20] Some experiments also showed that in physiological conditions, the complex is relatively labile and undergoes stepwise hydrolysis for two chlorides in two steps[6,22] and transforms into the corresponding more reactive aquated species.[20,23] Moreover, the hydrolysis process can be easily monitored spectrophotometriccally.[20] Apparently, the loss of two coordinated chlorides is the prerequisite for any further reactivity.[23] The resulting bis-aquated species may bind to various biomolecular targets, and thus it is very likely respon-

* Corresponding authors. E-mail: ceszkc@mail.sysu.edu.cn (Zheng); cesjln@mail.sysu.edu.cn (Ji). Tel: 0086-20-84110696. Fax: 0086-20-84112245.

† Sun Yat-Sen University.

‡ Tongji University.

10.1021/jp0711794 CCC: $37.00
Published on Web 06/19/2007

SCHEME 1: Proposed Hydrolysis of NAMI-A in Physiological Conditions

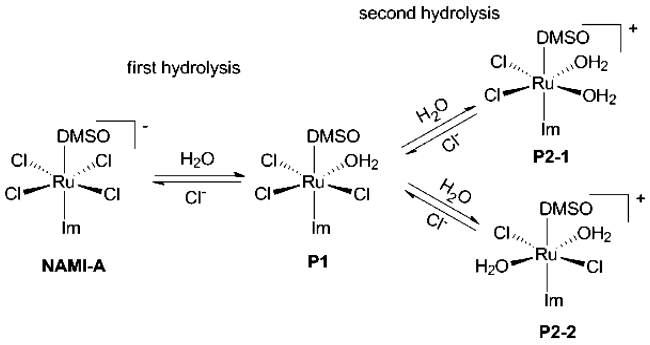

sible for the biological effects of NAMI-A.[24] However, the final biomolecular target and the activity mechanism of NAMI-A are largely unknown yet, and some controversial opinions still exist on this issue.[14,25] It is generally accepted that the hydrolysis process is the key activation step inside the cell before the drug reaches its intracellular target.

Many theoretical studies have been carried out in order to elucidate the basic step of the hydrolysis process of cisplatin and platinum-related complexes at different levels.[26−44] Particularly, more and more computations applying the DFT method to this field (the hydrolysis process of transition-metal-compound-type drugs) have been reported,[27,28,35,36,42] because DFT calculations consider electron correlation energies very well, obviously reduce the computational expenses.[45,46] However, as for ruthenium(III) drugs, especially for NAMI-A, although many experiments on activity characteristic and hydrolysis process as well as the patterns of binding to DNA have been well investigated,[14−25,47−49] to our knowledge, so far a comprehensive theoretical report on the hydrolysis mechanism of this kind of drug has not been found yet. A deeper insight into the aquation of NAMI-A is of importance for understanding the drug's function and its action within the cell and may be useful in the design of novel ruthenium(III)-based anticancer agents.

In this work, the first and second steps of the hydrolysis process of NAMI-A in physiological conditions (Scheme 1) are studied applying the density functional theory (DFT)[46,50−52] calculations. Related structures, thermodynamic properties, energies, and rate constants are calculated and discussed and compared with the available experimental results. Moreover, the solvent effects on the energies and kinetic properties for these reactions are also studied employing conductor-like polarizable continuum model (CPCM).[53−56]

II. Computational Methods

Since the central Ru(III) ion of NAMI-A has a d^5 electronic configuration in its valence shell, all geometry optimizations were carried out using density functional theory (DFT) UB3LYP approach, i.e., the unrestricted Becke three-parameter hybrid exchange functional[57](B3) and the Lee, Yang, and Parr (LYP) correlation functional.[58] The low ($S = 1/2$) spin state was employed, since the optimized structures of NAMI-A in high spin ($S = 5/2$) and intermediate spin ($S = 3/2$) states have not been obtained in our calculations. The LanL2DZ + 6-31G(d) hybrid basis set, i.e., the effective core potential basis set LanL2DZ[59−61] for Ru and the standard splitvalence basis set 6-31G(d)[62,63] for S, C, N, O, H, and Cl atoms, was used throughout this work for geometry optimizations and frequency calculations in vacuo. To obtain accurate energies for the reaction surfaces, single-point energies were further calculated

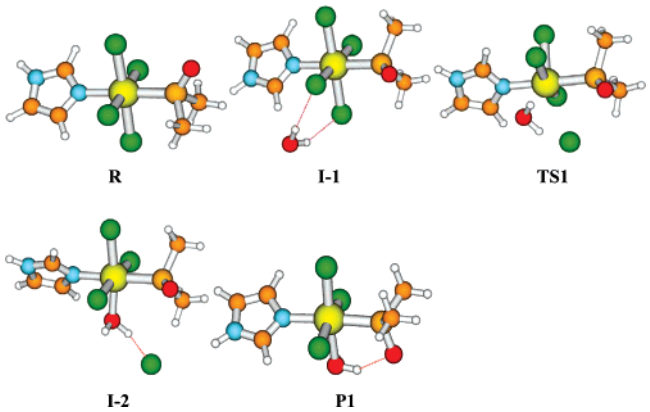

Figure 2. Optimized structures for the species involved in the first step of hydrolysis of NAMI-A.

in vacuo and in aqueous solution using the CPCM continuum solvation method[53−56] and using a higher basis set of LanL2DZ-(f) + 6-311++G(3df, 2pd), i.e., the LanL2DZ basis set including *f* polarization function ($\zeta_f = 1.235$)[64] was used for Ru (hereafter called LanL2DZ(f)), and 6-311++G(3df, 2pd) basis set was used for the other atoms. For the polarizable continuum-based solvation models of water, the CPCM method using UAKS cavities implemented in Gaussian 03 has been shown to be more accurate than PCM method.[65] In the CPCM method, the solute cavities are modeled on the optimized molecular shape, and include both electrostatic and nonelectrostatic contributions to the energies.[53,66]

Transition states (characterized by one imaginary frequency and one negative eigenvalue) were further confirmed by intrinsic reaction coordinate (IRC)[67−69]calculations. The reactant adduct and product adduct were obtained by following IRC of the corresponding transition state in both directions of the reaction path, followed by standard geometry optimizations. In all vacuum calculations, frequency calculations were carried out to verify the correct nature of the stationary points, and to extract the thermal energy contributions at 298.15 K and 1 atm. All calculations were performed using Gaussian 03 program packages.[70]

The activation Gibbs free energy was used to calculate the rate constants (k) through the transition state theory formalism[71] proposed by Eyring according to eq 1, where k_B is the Boltzmann constant, T is the absolute temperature, and h is the Planck constant. $\Delta G^{\ddagger}$ is the activation free energy for each step. The standard concentration (c °=1 mol/L) was considered:

$$k(T) = \frac{k_B T}{h} e^{-\Delta G^{\ddagger}/RT} \quad (1)$$

III. Results and Discussion

A. Structural Characteristics. The fully optimized structures for the species involved in the first step of the hydrolysis of the NAMI-A are shown in Figure 2, and those in the second step of the hydrolysis step are depicted in Figure 3. The selected structural parameters for the optimized stationary points are listed in Tables 1 and 2 for the first and second steps of hydrolysis, respectively, including reactants, intermediates, transition states, and products. The numbers of the atoms in Tables 1 and 2 and Figures 2 and 3 are shown in Figure 1. In general, the various structures presented in Figures 2 and 3 have many geometric features, but here only the most prominent characteristics are discussed; in particular, some features of the intermediates and transition states are emphasized.

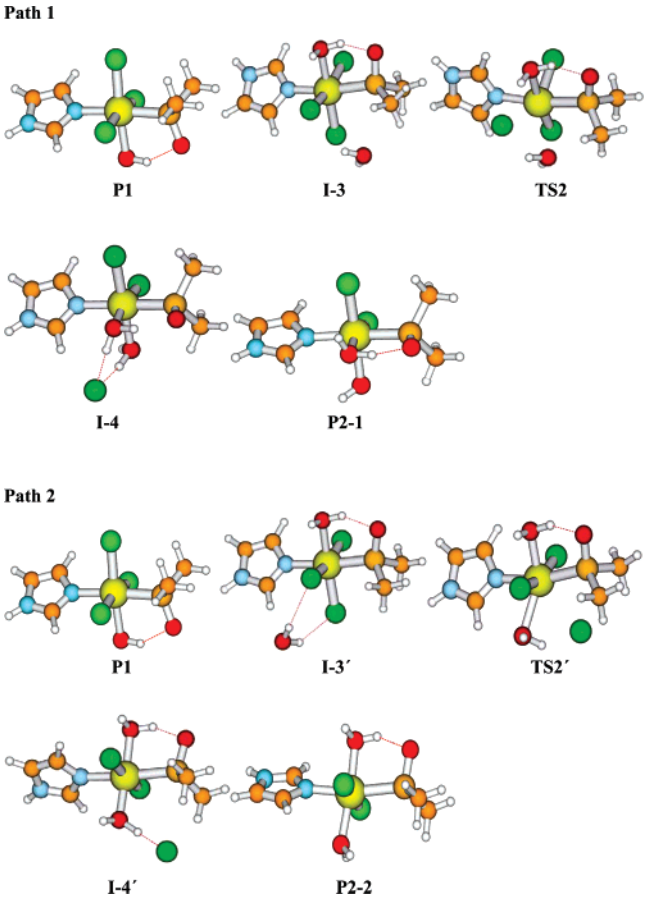

Figure 3. Optimized structures for the species involved in the second step of hydrolysis of NAMI-A.

TABLE 1: Optimized Geometric Parameters for All Stationary Points in the First Hydrolysis Reaction of NAMI-A at the Level of UB3LYP/(LanL2DZ + 6-31G(d)) (cf. Figure 1)

	first hydrolyzis step					
	NAMI-A[a]	NAMI[b]	**I-1**	**TS1**	**I-2**	**P1**
Cl2−Ru	2.43(2.46)	2.34	2.45	2.99	4.69	
Cl3−Ru	2.44(2.43)	2.32	2.46	2.55	2.42	2.43
Cl4−Ru	2.40(2.40)	2.36	2.42	2.40	2.39	2.39
Cl5−Ru	2.46(2.43)	2.34	2.42	2.43	2.41	2.36
N6−Ru	2.10(2.09)	2.08	2.11	2.10	2.10	2.10
S7−Ru	2.41(2.40)	2.30	2.42	2.42	2.42	2.36
O(wat1)−Ru			4.30	2.56	2.14	2.21
Cl2−Ru−Cl3	89.3(89.3)	90.8	89.5	117.0		
Cl2−Ru−Cl4	178.0(178.0)	179.1	179.1	153.9		
Cl2−Ru−Cl5	90.1(90.1)	90.2	90.1	75.0		
Cl2−Ru−N6	89.5(89.5)	89.6	89.4	107.0		
Cl2−Ru−S7	88.9(88.9)	87.4	88.6	73.8		
Cl3−Ru−Cl4	90.9(90.8)	89.3	90.3	82.8	92.9	97.3
Cl3−Ru−Cl5	177.2(177.2)	176.0	178.3	167.0	171.6	167.1
Cl4−Ru−Cl5	89.6(89.7)	89.7	90.0	84.2	95.2	95.6
Cl5−Ru−N6	88.5(88.5)	87.7	88.6	86.0	89.6	89.1
Cl5−Ru−S7	91.2(91.2)	91.5	91.1	96.5	89.2	90.6
S7−Ru−N6	178.4(178.4)	176.9	178.0	177.6	178.9	176.5
O(wat1)−Ru−Cl2			49.3	62.0		
O(wat1)−Ru−Cl3			49.1	69.8	83.1	86.1

[a] The data in parentheses are the geometrical parameters calculated at UB3LYP/(LanL2DZ(f) + 6-31G(d)) level. [b] The experimental values come from the X-ray structure of analogue NAMI;[72] NAMI is Na[*trans*-$RuCl_4$(DMSO)(Im)].

In general, the changes in the bond lengths of the ligands not directly involved in the reaction are only marginal among the different states. All reactant and product complexes have pseudooctahedral coordination around the Ru atom. The water molecules form hydrogen bonds with the negative chlorides or DMSO group. Forming of hydrogen bonds makes all reactant and product complexes not be perfectly octahedrons (except the reactant molecule **R**), the central axis is somewhat skew as shown in Figures 2 and 3.

1. First Hydrolysis Step. From Figure 2 and Table 1, it can be seen that the reactant molecule (NAMI-A, **R**) is pseudooctahedral configuration with four equatorial chloride ligands, and DMSO and imidazole as axial ligands. The Ru−Cl bond length is within the range of 2.40−2.46 Å, Ru−N and Ru−S bond lengths are 2.10 and 2.41 Å, respectively. Comparing the computed results of NAMI-A with the experimental data of NAMI[72] (see in Table 1), we can find that all of the computed selective bond lengths are slightly longer than the corresponding experimental ones. The computational differences from the experimental data can be thought as systematic errors caused by the computation method/basis set and environment factors. Therefore, the results of the full geometry optimization computations by the DFT method at UB3LYP/(LanL2DZ + 6-31G(d)) level should be reliable, and based on the computed geometries of the complexes, we can carry out the study on the structures as well as the further study on energies, thermodynamic and kinetic properties for the hydrolysis of NAMI-A at higher basis set level.

In the first intermediate, $[RuCl_3(DMSO)(Im)]^{-1}...H_2O$, **I-1**, the entering water molecule has formed hydrogen bonds with two adjacent Cl atoms with the distances $R(Cl2-H_{wat}) = 2.39$ Å and $R(Cl3-H_{wat}) = 2.40$ Å. The transition state (**TS1**) structure found for the first hydrolysis step is characterized by an imaginary frequency of 138 cm^{-1}, in which the Ru−Cl2 bond is breaking and the Ru−O (wat1) bond is forming, and the other three Cl atoms are forming a plane perpendicular to the central axis. The distance between Ru and O atom of the entering water molecule reduces from 4.30 Å in **I-1** to 2.56 Å in **TS1**, while the Ru-Cl2 distance increases from 2.45 to 2.99 Å. In the structure of intermediate **I-2**, $[RuCl_3(H_2O)(DMSO)(Im)]...Cl^-$, the Cl atom as ligand has been completely substituted by H_2O which forms a bond with Ru at distance of 2.14 Å, resulting in a pseudooctahedral geometry. The Cl atom forms intermolecular interactions with H atom of the coordinated water molecule at distance of 1.87 Å. The first step hydrolysis product **P1** has a pseudooctahedral configuration, in which the leaving Cl2 has been removed from the system, and the coordinated water molecule forms a hydrogen bond (1.86 Å) with O atom of DMSO group.

2. Second Hydrolysis Step. Two paths are found in the second hydrolysis process. In the path 1, the second entering water molecule replaces the Cl atom as ligand at the cis-position of the first coordinated water molecule; and in the path 2, the second entering water molecule replaces the Cl atom as ligand at the trans-position of the first coordinated water molecule. The optimized structures found for the second hydrolysis step are shown in Figure 3. In the path 1, the distance between the attacking O atom and Ru atom is 4.29 Å. The transition state structure found in path 1, **TS2** is characterized by an imaginary frequency of 131 cm^{-1}, in which the forming Ru−O(wat2) bond is 2.64 Å and the breaking Ru−Cl5 bond is 2.86 Å. The structure of **TS2** is similar to that of **TS1**, i.e., the bond length of Ru−O(wat2) reduces and the Ru−Cl5 distance correspondingly increases. In the intermediate **I-4**, the bond length Ru−O(wat2) is 2.18 Å, and the expelled Cl^- ion lies at a distance of 4.02 Å from the Ru atom. It is noted that the Cl^- ion forms two hydrogen bonds with the two bound water ligands at distances 1.99 and 1.92 Å, respectively.

TABLE 2: Optimized Geometric Parameters for All Stationary Points in the Second Hydrolysis Reaction of NAMI-A at the Level of UB3LYP (LanL2DZ + 6-31G(d)) (cf. Figure 1)

	path 1				path 2			
	I-3	**TS2**	**I-4**	**P2-1**	**I-3′**	**TS2′**	**I-4′**	**P2-2**
Cl3−Ru	2.38	2.35	2.37	2.31	2.37	2.38	2.38	2.37
Cl4−Ru	2.36	2.42	2.34	2.34	2.36	2.95	4.21	
Cl5−Ru	2.43	2.86	4.02		2.45	2.52	2.41	2.36
N6−Ru	2.10	2.09	2.11	2.11	2.10	2.11	2.11	2.08
S7−Ru	2.38	2.42	2.38	2.40	2.38	2.45	2.44	2.49
O(wat1)−Ru	2.20	2.21	2.12	2.17	2.19	2.14	2.15	2.10
O(wat2)−Ru	4.29	2.64	2.18	2.23	4.27	2.41	2.05	2.16
Cl3−Ru−Cl4	95.7	88.2	97.0	100.1	96.7	80.3	94.1	
Cl3−Ru−Cl5	168.1	145.0	133.1		168.5	163.0	174.2	170.8
Cl3−Ru−N6	89.8	87.0	89.3	88.8	89.6	86.1	89.7	91.8
Cl3−Ru−S7	88.6	87.5	90.6	91.0	89.4	89.4	88.7	88.6
Cl4−Ru−Cl5	96.1	122.3	127.0		94.8	113.5		
S7−Ru−N6	174.7	171.9	176.9	174.4	174.7	166.6	174.7	170.8
O(wat1)−Ru−Cl3	85.5	81.4	91.8	90.0	87.2	84.7	89.2	94.9
O(wat2)−Ru−Cl4	50.4	70.2	84.8	84.2	52.1	62.5		
O(wat2)−Ru−Cl5	54.2	63.6			52.1	73.1	91.8	87.9

The final product complex (**P2−1**), i.e., the double aquated species of NAMI-A produced according to the path 1, shows a pseudooctahedral geometry. The hydrolysis mode and structural characters of the species in the path 2 are similar to those in the path 1. The final product complex (**P2−2**) in the path 2 and **P2−1** are isomeric.

In order to vividly depict structural variations during the hydrolysis process, the important bond lengths on the reaction center for the reactant, transition state, intermediate and product in the first and second hydrolysis steps are plotted in Figure 4.

In summary, the second hydrolysis step exhibits the similar geometric features to the first hydrolysis step. The structural data in Tables 1 and 2 show that the geometric changes

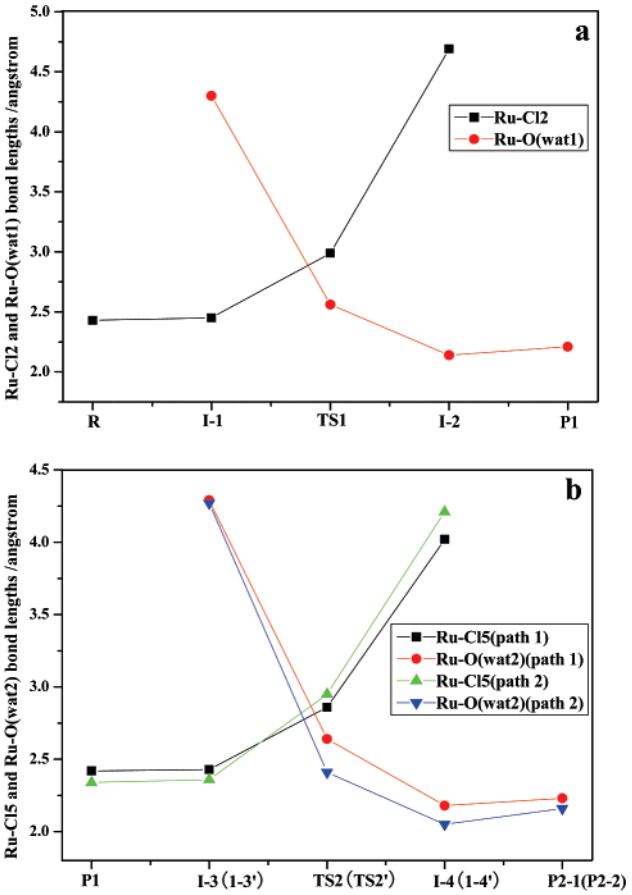

Figure 4. Ru−Cl and Ru−O bond length variation for the first (a) and second (b) steps of the hydrolysis process of the NAMI-A.

associated with the hydrolysis mainly take place on the equatorial plane of octahedron according to the DFT calculations. The above analysis demonstrates that the hydrolysis modes and structural characteristics of stationary states of NAMI-A are in accordance with those of other transition metal complexes, e.g., cisplatin[27,28,34,41] and its analogues.[28,42,44]

3. Electronic Characteristics. In order to obtain more electronic information for these hydrolysis reactions, the natural orbital population analysis (NPA)[46,73] was carried out, and the net charges of important atoms for every stationary point were listed in Table 3. Corresponding to the geometric structural changes in the hydrolysis process, the most remarkable variations of atomic net charges also occur in the three atoms which directly relate to the reactions, i.e., the central Ru atom, the leaving Cl atom, and the attacking O atom. Among these three atoms, Ru and Cl show the largest charge variation, in agreement with the largest bond length variation of R_{Ru-Cl}, whereas the O atom of the entering water molecule presents a smaller charge change due to the smaller change of R_{Ru-O}. The trend in the charge changes can be clearly seen in Figure 5. With the reaction proceeding, the net charge of the Cl^- ion as leaving ligand (Q_{Cl}) becomes more negative, the positive charge of the central Ru atom (Q_{Ru}) increases first and then reduces because of receiving some negative charges after TS. This phenomenon indicates that there is a charge transfer among the related atoms, and that the negative charge gain of the Cl atom is greater than the negative charge loss of the Ru atom. In fact, in the first hydrolysis step, the negative charge on leaving Cl^- ion increases by 0.281 |e| (from −0.505 to −0.786 |e|), but the positive charge on Ru atom increases by 0.047 |e| (from 0.472 to 0.519 |e|). To meet the charge conservation of the hydrolysis reaction, the negative charge of O atom of the entering water ligand, decreases to favor the nucleophilic attack in the formation of a relatively stable intermediate complex. A similar electronic characteristic of hydrolysis process was also found for cisplatin and its analogues,[28] showing the same reaction pathway, i.e., second-order nucleophilic substitution (S_N2) reaction.[42,44,74]

B. Reaction Profiles of the Hydrolysis Processes. To quantitatively assess the hydrolysis behaviors of NAMI-A, various kinds of energetic terms were computed with the incorporation of thermal effects at 298.15 K. The computed relative energies of the intermediate species and transition states of the first and second hydrolysis processes along with their solvation energies, entropies, thermal corrections to the enthalpies, and the resultant relative enthalpies and the free energies in aqueous solution at 298.15 K are given in Table 4. On the

TABLE 3: Atomic Net Charge Populations of Central Ru(III) Atom, Leaving Cl Ion, and Attacking O Atom of Each Hydrolysis Step (Unit: |e|)

		R	I-1	TS1	I-2	P1
first hydrolysis step	Ru	0.4718	0.4879	0.5815	0.5780	0.5189
	Cl2	−0.5052	−0.5313	−0.6704	−0.7863	
	O(wat1)		−0.9914	−0.9508	−0.9273	−0.8957
second hydrolysis step		**P1**	**I-3(I-3′)**	**TS2(TS2′)**	**I-4(I-4′)**	**P2-1(P2-2)**
path 1	Ru	0.5189	0.5375	0.6382	0.6544	0.6190
	Cl5	−0.4973	−0.5134	−0.6424	−0.6999	
	O(wat2)		−0.9619	−0.9577	−0.9331	−0.9038
path 2	Ru	0.5189	0.5410	0.7245	0.7094	0.7001
	Cl4	−0.3778	−0.4133	−0.6316	−0.6959	
	O(wat2)		−0.9649	−0.9418	−0.8742	−0.8738

basis of these results, the potential energy surfaces corresponding to the first and second aquation processes are displayed in Figures 6, 7, and 8, respectively.

The ZPE-corrected energy profiles computed in the gas phase, $\Delta E_{tot/ZEP}(g)$, are displayed in Figure 6. Several significant features can be found from Figure 6, according to the order of the first hydrolysis step, the path 1 and path 2 in the second hydrolysis step, the barrier heights are 31.8, and 22.6, 34.0 kcal/mol, respectively, demonstrating the path 2 of the second step is more difficult than the path 1 and the first step. The same sequence of barrier heights also can be seen in Figures 7 and 8. Figure 6 shows that all the reactions can be quantitatively predicted to be endothermic by 6.3, and 1.0, 10.9 kcal/mol, respectively, and further suggests that the path 2 in the second hydrolysis step is a difficult reaction path. Comparing $\Delta E_{tot/ZEP}(g)$ with $\Delta E_{tot}(g)$ in Table 4, it is easy to see that the inclusion of ZPE-corrected energy has a very minor effect on all the reaction species, in which the largest change occurs in **1**−**4′** (energy reduced by 0.8 kcal/mol).

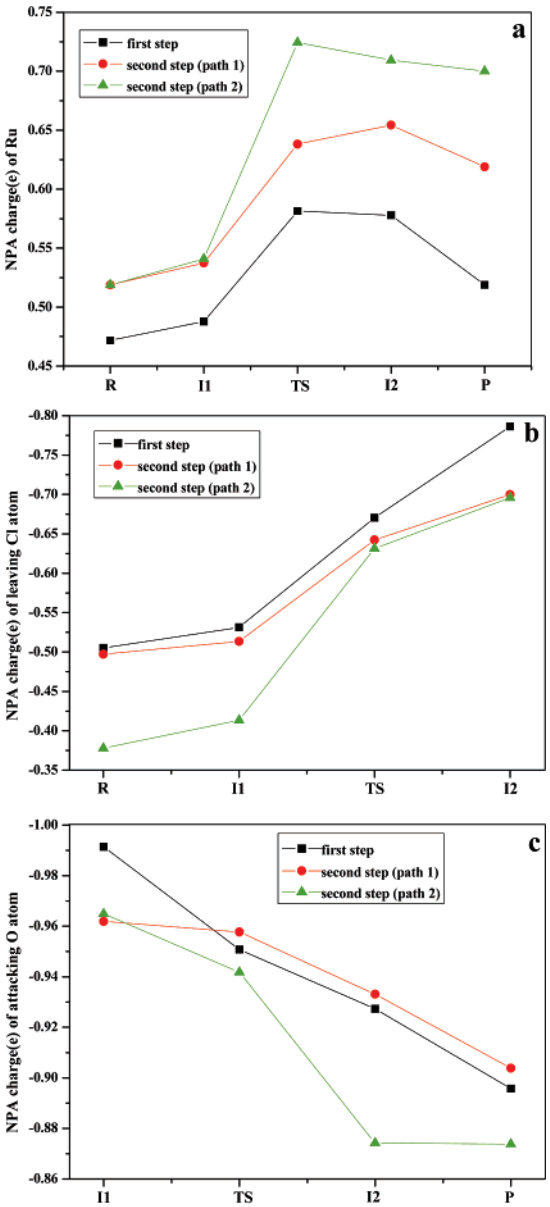

Figure 5. NPA charges of the three important atoms, (a) the central Ru atom, (b) the leaving Cl atom, (c) the attacking O atom, in each hydrolysis step.

In Figure 7, the single-point energies calculated using CPCM solvation model in aqueous solution with the higher combined basis set of LanL2DZ(f) + 6-311++G(3df, 2pd), are displayed. Several features can be observed from the reaction profiles after accounting for the solvent effect: (1) The barrier heights decrease to 26.9, 22.2 and 30.2 kcal/mol, for the first step and the path 1 and path 2 of the second step, respectively, relative to their gas-phase values 31.8, 22.6 and 34.0 kcal/mol. (2) In contrast to the gas-phase reaction, the reactions of the first hydrolysis step and the path 1 of the second step in aqueous solution are predicted to be exothermic by 1.3 and 1.7 kcal/mol, but the path 2 is still endothermic ($\Delta E_{tot}(aq) = 1.6$ kcal/mol) due to its higher barrier height.

In Figure 8, we presented the computed relative free energies for the aqueous reactions in solution. Comparing them with the energy data in Figure 7, we find the following: the free energies display slightly lower barriers (by 0.1−3.7 kcal/mol) and all of these hydrolysis steps and paths are exothermic. Moreover, the computed free energy barrier of the first hydrolysis step of NAMI-A is 23.2 kcal/mol, in excellent agreement with the experimental activation energy[47] which was measured to be 95.4 kJ/mol (22.8 kcal/mol) in the temperature range 4−37 °C.

In addition, it is found that the path 2 is more difficult than the path 1 both in gas phase and aqueous solution for the second hydrolysis reaction. It can be reasonably explained by the total energies of the final product complexes **P2**−**1** and **P2**−**2** obtained from calculations (see Table 5). Table 5 shows that both the calculated ZPE-corrected total energy in gas phase ($E_{tot/ZEP}(g)$) and the total energy in aqueous solution ($E_{tot}(aq)$) of **P2**−**1** are lower than those of **P2**−**2**. Therefore, it suggests that **P2**−**1** is thermodynamically more stable than **P2**−**2**.

From the barrier heights shown in the reaction profiles of hydrolysis processes of NAMI-A (see in Figures 6, 7, and 8), we can see that the reactions in aqueous solution are mainly exothermic. In addition, solvent effects are more important for the energetics than the zero-point vibrational effects (ZPE) and make the free energies reduce. For the hydrolysis reactions, since the path 2 is more difficult than the path 1 and the first step, we can reasonably suggest that the hydrolysis process of NAMI-A perform mainly via the first hydrolysis step and then

TABLE 4: Relative Gas-Phase Energies, Total and Relative Solvation Energies, Thermal Contributions to Enthalpies, Standard Entropies, Relative Enthalpies, and Gibbs Free Energies at 298.15 K for All Intermediate Species and Transition States of the First and the Second Aquation Processes[a,b]

species	ΔE_{tot}(g)	$\Delta E_{tot/ZPE}$(g)	G_{solv}[c]	ΔE_{tot}(aq)	G_{therm}[d]	H_{therm}[d]	$\Delta H°$(aq)	$\Delta S°$	$\Delta G°$(g)	$\Delta G°$(aq)	K(g)	K(aq)
I-1	0	0	−55.7	0	84.3	131.3	0	0	0	0		
TS1	32.4	31.8	−63.5	26.9	84.6	130.3	23.0	−0.6	31.0	23.2	1.17×10^{-10}	6.11×10^{-5}
I-2	6.7	6.3	−65.3	−1.3	84.2	130.5	−4.2	1.2	5.1	−4.6		
						path 1						
I-3	0	0	−12.3	0	100.0	147.3	0	0	0	0		
TS2	22.5	22.6	−13.6	22.2	100.9	146.6	20.5	−5.1	23.4	22.1	4.36×10^{-5}	3.30×10^{-4}
I-4	0.9	1.0	−16.8	−1.7	101.0	146.6	−4.2	−5.7	2.1	−2.5		
						path 2						
I-3′	0	0	−10.3	0	100.6	147.5	0	0	0	0		
TS2′	33.9	34.0	−18.0	30.2	101.6	146.6	25.4	−6.4	35.0	27.3	1.37×10^{-13}	6.03×10^{-8}
I-4′	11.7	10.9	−24.3	1.6	100.1	145.9	−4.6	−3.5	10.4	−3.6		

[a] All energy values in kcal/mol and $\Delta S°$ in cal K^{-1} mol^{-1}. [b] E_{tot}, the single-point energy calculated at the level of UB3LYP/(LanL2DZ(f) + 6-311++G(3df, 2pd)) on structures optimized at the UB3LYP/(LanL2DZ + 6-31G(d)) level, total enthalpies, and Gibbs free energies (including solvation and zero-point energy) were obtained as follows: $H°(aq) = E_{tot/ZPE}(g) + G_{solv} + H_{therm}$; $G°(aq) = E_{tot/ZPE}(g) + G_{solv} + G_{therm}$; $G°(aq) = H°(aq) - 298.15\ S°$. [c] The solvation energy corrections to the single-point energies calculated using the CPCM solvation model at the level of UB3LYP/(LanL2DZ(f) + 6-311++G(3df, 2pd)). [d] Thermal correction obtained through frequency calculation at the level of UB3LYP/(LanL2DZ + 6-31G(d)) at 298.15 K and 1 atm on the optimized stationary point geometries.

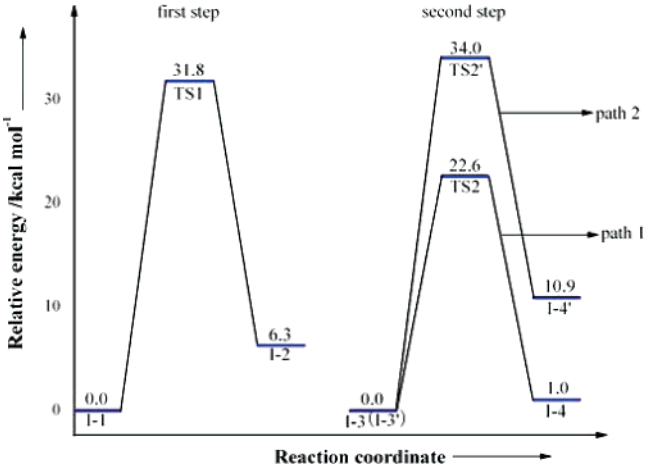

Figure 6. Energetic profiles of the first and second hydrolysis steps of NAMI-A in the gas phase.

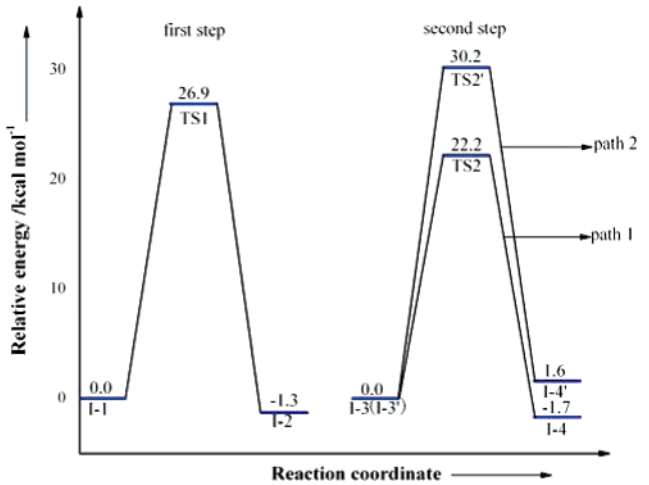

Figure 7. Energetic profiles of the first and second hydrolysis steps of NAMI-A in aqueous phase.

the path 1 of the second hydrolysis step, and thus that the diaquated product of the path 2 (**P2−2**) should be less frequent than that of the path 1(**P2−1**).

C. Kinetic Analysis. The rate constants were calculated within the transition state theory formalism,[70] using the Eyring equation [eq 1]. The results are displayed in Table 4. The value

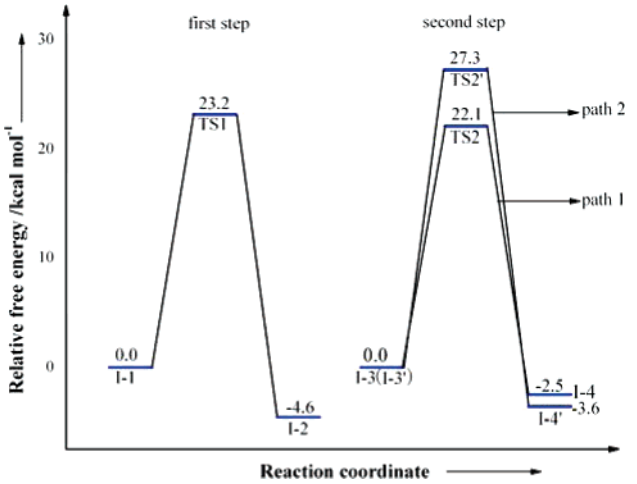

Figure 8. Free energy profiles of the first and second hydrolysis steps of NAMI-A in aqueous phase.

TABLE 5: The Gas-Phase ZPE-Corrected Energies and the Aqueous-Phase Single-Point Energies of the Second Hydrolysis Products P2-1 and P2-2

	$E_{tot/ZEP}$(g) (au)	E_{tot}(aq) (au)
P2-1	−1946.6044	−1946.9176
P2-2	−1946.6019	−1946.9152
Δ[a]	1.52 kcal/mol	1.50 kcal/mol

[a] The energy difference between **P2-2** and **P2-1**, i.e., $\Delta = E_{P2-2} - E_{P2-1}$.

obtained for the first step (6.11×10^{-5} s^{-1}) in aqueous solution is close to the experimental values, which are $2.77 \times 10^{-8} - 1.44 \times 10^{-5}$ s^{-1} in different buffer concentration (pH 5−8)[47] and 5.58×10^{-6} in phosphate buffer (pH 7.4) exposed to light.[49] Since the rate constants calculated in gas phase show smaller (1.17×10^{-10} s^{-1}), it further shows that the importance of solvent effect on the hydrolysis of NAMI-A. For the second hydrolysis process, although so far the explicit experimental data able to use to compare with the theoretical ones are not found yet, some experimental results[22] suggested that the hydrolysis of the second chloride be slower than that of the first one and occurs in approximately 2 h at 25 °C. It seems to be inconsistent with our calculation results for the second hydrolysis step (path 1). The disagreement may be attributed to the effect of solvent or solvent model. It has been reported

that in the hydrolysis process, the energy values are sensitive to the different types of solvent as well as the sizes and structures of the hydrolysis model.[35,36]

For the hydrolysis process of cisplatin and its analogs, the theoretical studies have been reported since the nineties of 20th century, and the theoretical methods and model are mature and experiential. With respect to the drug NAMI-A (Ru(III)-based anticancer agent), the mechanism of hydrolysis process, especially the second step is very complicated, and some controversial opinions unavoidably exist.[14,25] Moreover, the structure and activation mechanism of Ru(III)-based anticancer agents are different from that of cisplatin and its analogs, thus the theoretical model for cisplatin may be not fit for NAMI-A. Since the theoretical study on this field has just started, to explore and design more accurate solvent model for the hydrolysis of NAMI-A is a very important and difficult work. However, our limited quantum-chemical studies provide the structural properties and detailed energy profiles for the mechanism of hydrolysis of NAMI-A, which may contribute to understanding the reaction mechanism of this drug with the biomolecular target. Besides, the present work may give a new insight to further designing accurate solvent model for the hydrolysis process of the title compound, and thus our further work on this field is in progress.

IV. Conclusions

In the present work, the hydrolysis processes of the anticancer drug NAMI-A have been investigated by using the quantum chemistry DFT method. The related geometries and vibrational frequencies during the hydrolysis processes were obtained at the UB3LYP/(LanL2DZ + 6-31G(d)) level in the gas phase, followed by exact single-point energy calculations performed at the UB3LYP/(LanL2DZ(f)+6-311++G(3df,2dp) level both in vacuo and in aqueous solution using the CPCM model. The theoretical results show the following: (1) The structures of the transition states have pseudooctahedral geometries. The geometric changes associated with the reaction processes mainly take place in the equatorial plane of the pseudooctahedral geometry. (2) For the first hydrolysis process, the computed relative free energies $\Delta G°$ (aq) and rate constant (k) in aqueous solution are 23.2 kcal/mol and 6.11×10^{-5} s^{-1}, respectively, in satisfactory agreement with the experimental values. (3) It is found that the solvent effects play an important role than the zero-point vibrational effects (ZPE) in the energetics of title compound. In particular, for the second hydrolysis step, some disagreement still exists and thus more accurate solvent model needs to be designed. (4) On the basis of our present limited work, it can reasonably suggest that the hydrolysis process of NAMI-A performs mainly via the first hydrolysis step and then the path 1 of the second hydrolysis step.

Acknowledgment. The financial supports of the National Natural Science Foundation of China, the Natural Science Foundation of Guangdong Province and the Research Fund for the Doctoral Program of Higher Education of China are gratefully acknowledged.

References and Notes

(1) Rosenberg, B. In *Cisplatin. Chemistry and Biochemistry of a Leading Anticancer Drug*; Lippert, B., Ed.; Wiley-VCH: Zürich, 1999; p 3.

(2) O'Dwyer, P. J.; Stevenson, J. P.; Johnson, S. W. In *Cisplatin. Chemistry and Biochemistry of a Leading Anticancer Drug*; Lippert, B., Ed.; Wiley-VCH: Zürich, 1999; p 31.

(3) Wong, E.; Giandomenico, C. M. *Chem. Rev.* **1999**, *99*, 2451.

(4) Clarke, M. J. In *Metal Complexes in Cancer Chemotherapy*; Keppler, B. K., Ed.; VCH: Weinheim, Germany, 1993; p 129.

(5) Keppler, B. K.; Lipponer, K.-G.; Stenzel, B.; Kratz, F. In *Metal Complexes in Cancer Chemotherapy*; Keppler, B. K., Ed.; VCH: Weinheim, Germany, 1993; p 187.

(6) Clarke, M. J.; Zhu, F.; Frasca, D. R. *Chem. Rev.* **1999**, *99*, 2511.

(7) Sava, G.; Bergamo, A. *Int. J. Oncol.* **2000**, *17*, 353.

(8) Aird, R. E.; Cummings, J.; Ritchie, A. A.; Muir, M.; Morris, R. E.; Chen, H.; Sadler, P. J.; Jodrell, D. I. *Br. J. Cancer* **2002**, *86*, 1652.

(9) Morris, R. E.; Aird, R. E.; Del Socorro Murdoch, P.; Chen, H.; Cummings, J.; Hughes, N. D.; Parsons, S.; Parkin, A.; Boyd, G.; Jodrell, D. I.; Sadler, P. J. *J. Med. Chem.* **2001**, *44*, 3616.

(10) Hotze, A. C. G.; Caspers, S. E.; de Vos, D.; Kooijman, H.; Spek, A. L.; Flamigni, A.; Bacac, M.; Sava, G.; Haasnoot, J. G.; Reedijk, J. *J. Biol. Inorg. Chem.* **2004**, *9*, 354.

(11) Velders, A. H.; Kooijman, H.; Spek, A. L.; Haasnoot, J. G.; de Vos, D.; Reedijk, J. *Inorg. Chem.* **2000**, *39*, 2966.

(12) Van Vliet, P. M.; Sarinten, M. S.; Toekimin, S. M. S.; Haasnoot, J. G.; Reedijk, J.; Nováková, O.; Vrána, O.; Brabec, V. *Inorg. Chim. Acta*. **1995**, *231*, 57.

(13) Hotze, A. C. G.; Bacac, M.; Velders, A. H.; Jansen, B. A. J.; Kooijman, H.; Spek, A. L.; Haasnoot, J. G. and Reedijk, J. *J. Med. Chem.* **2003**, *46*, 1743.

(14) Sava, G.; Alessio, E.; Bergamo, A.; Mestroni, G. In *Topics in Biological Inorganic Chemistry*; Clarke, M. J., Sadler, P. J., Eds.; Springer: Berlin, 1999; p 143.

(15) Sava, G.; Capozzi, I.; Clerici, K.; Gagliardi, R.; Alessio, E.; Mestroni, G. *Clin. Exp. Metastasis* **1998**, *16*, 371.

(16) Sava, G.; Clerici, K.; Capozzi, I.; Cocchietto, M.; Gagliardi, R.; Alessio, E.; Mestroni, G.; Perbellini, A. *Anti-Cancer Drugs* **1999**, *10*, 129.

(17) Bergamo, A.; Zorzet, S.; Gava, B.; Sorc, A.; Alessio, E.; Iengo, E.; Sava, G. *Anti-Cancer Drugs* **2000**, *11*, 667.

(18) Cocchietto, M.; Sava, G. *Pharmacol. Toxicol.* **2000**, *87*, 193.

(19) Sava, G.; Cocchietto, M. *In Vivo* **2000**, *14*, 741.

(20) Mestroni, G.; Alessio, E.; Sava, G.; Pacor, S.; Coluccia, M.; Bocarelli, A. *Metal Based Drugs* **1994**, *1*, 41.

(21) Sava, G.; Alessio, E.; Bergamo, A.; Mestroni, G. In *Biological Inorganic Chemistry*; Clarke, M. J., Sadler, P. J., Eds.; Springer-Verlag: Berlin, 1999; Vol. 1, p 154.

(22) Savaa, G.; Bergamoa, A.; Zorzetb, S.; Gavaa, B.; Casarsaa, C.; Cocchiettoa, M.; Furlanib, A.; Scarciab, V.; Serlic, B.; Iengoc, E.; Alessioc, E.; Mestronic, G. *Eur. J. Cancer* **2002**, *38*, 427.

(23) Messori, L.; Kratz, F.; Alessio, E. *Metal Based Drugs* **1996**, *3*, 1.

(24) Messori, L.; Orioli, P.; Vullo, D.; Alessio, E.; Iengo, E. *Eur. J. Biochem.* **2000**, *267*, 1206.

(25) Sava, G.; Capozzi, I.; Bergamo, A.; Gagliardi, R.; Cocchietto, M.; Masiero, L.; Onisto, M.; Alessio, E.; Mestroni, G.; Garbisa, S. *Int. J. Cancer* **1996**, *68*, 60.

(26) Burda, J. V.; Zeizinger, M.; Sponer, J.; Leszczynski, J. *J. Chem. Phys.* **2000**, *113*, 2224.

(27) Chval, Z.; Sip, M. *J. Mol. Struct.* (*THEOCHEM*) **2000**, *532*, 59.

(28) Zhang, Y.; Guo, Z. J.; You, X. Z. *J. Am. Chem. Soc.* **2001**, *123*, 9378.

(29) Zeizinger, M.; Burda, J. V.; Sponer, J.; Kapsa, V.; Leszczynski, J. *J. Phys. Chem. A* **2001**, *105*, 8086.

(30) Cooper, J.; Ziegler, T. *Inorg. Chem.* **2002**, *41*, 6614.

(31) Raber, J.; Llano, J.; Eriksson, L. A. In *Quantum Medicinal Chemistry*; Carloni, P., Alber, F., Eds.; Wiley-VCH: Weinheim, Germany, 2003; p 113.

(32) Robertazzi, A.; Platts, J. A. *J. Comput. Chem.* **2004**, *25*, 1060.

(33) Burda, J. V.; Zeizinger, M.; Leszczynski, J. *J. Chem. Phys.* **2004**, *120*, 1253.

(34) Raber, J.; Zhu, C.; Eriksson, L. A. *Mol. Phys.* **2004**, *102*, 2537.

(35) Song, T.; Hua, P. *J. Chem. Phys.* **2006**, *125*, 091101.

(36) Hush, N. S.; Schamberger, J.; Bacskay, G. B. *Coord. Chem. Rev.* **2005**, *249*, 299.

(37) Burda, J. V.; Zeizinger, M.; Leszczynski, J. *Comput. Chem.* **2005**, *26*, 907.

(38) Carloni, P.; Sprik, M.; Andreoni, W. *J. Phys. Chem. B* **2000**, *104*, 823.

(39) Lau, J. K.-C.; Deubel, D. V. *J. Chem. Theory Comput.* **2006**, *2*, 103.

(40) Cundari, T. R.; Fu, W. *J. Mol. Struct.: THEOCHEM* **1998**, *425*, 51.

(41) Carloni, P.; Andreoni, W.; Hutter, J.; Curioni, A.; Giannozzi, P.; Parrinello, M. *Chem. Phys. Lett.* **1995**, *234*, 50.

(42) Zhu, C.-B.; Raber, J.; Eriksson, L. A. *J. Phys. Chem. B* **2005**, *109*, 12195.

(43) Raber, J.; Zhu, C.-B.; Eriksson, L. A. *J. Phys. Chem. B* **2005**, *109*, 11006.

(44) SodréCosta, L. A.; Rocha, W. R.; De Almeida, W. B.; Dos Santos, H. F. *J. Chem. Phys.* **2003**, *118*, 10584.

(45) Kurita, N.; Kobayashi, K. *Comput. Chem.* **2000**, *24*, 351.

(46) Foresman, J. B.; Frisch, Æ. In *Exploring Chemistry with Electronic Structure Methods*, 2nd ed.; Gaussian Inc.: Pittsburgh, PA, 1996).

(47) Bouma, M.; Nuijen, B.; Jansen, M. T.; Sava, G.; Flaibani, A.; Bult, A.; Beijnen, J. H. *Int. J. Pharm.* **2002**, *248*, 239.
(48) Bouma, M.; Nuijen, B.; Jansen, M. T.; Sava, G.; Picotti, F.; Flaibani, A.; Bult, A.; Beijnen, J. H. *J. Pharm. Biomed. Anal.* **2003**, *31*, 215.
(49) Bouma, M.; Nuijen, B.; Jansen, M. T.; Sava, G.; Picotti, F.; Flaibani, A.; Bult, A.; Beijnen, J. H. *J. Pharm. Biomed. Anal.* **2002**, *30*, 1287.
(50) Hohenberg, P.; Kohn, W. *Phys. Rev. B* **1964**, *136*, 864.
(51) Becke, A. D. *J. Chem. Phys.* **1993**, *98*, 1372.
(52) Görling, A. *Phys. Rev. A* **1996**, *54*, 3912.
(53) Barone, V.; Cossi, M. *J. Phys. Chem. A* **1998**, *102*, 1995.
(54) Cossi, M.; Rega, N.; Scalmani, G.; Barone, V. *J. Comput. Chem.* **2003**, *24*, 669.
(55) Klamt, A.; Schüürmann, G. *J. Chem. Soc., Perkin Trans.* **1993**, *2*, 799.
(56) Andzelm, J.; Kölmel, C.; Klamt, A. *J. Chem. Phys.* **1995**, *103*, 9312.
(57) Becke, A. D. *J. Chem. Phys.* **1993**, *98*, 5648.
(58) Lee, C.; Yang, W.; Parr, R. G. *Phys. Rev. B* **1988**, *37*, 785.
(59) Hay, P. J.; Wadt, W. R. *J. Chem. Phys.* **1985**, *82*, 270.
(60) Wadt, W. R.; Hay, P. J. *J. Chem. Phys.* **1985**, *82*, 284.
(61) Wadt, W. R.; Hay, P. J. *J. Chem. Phys.* **1985**, *82*, 299.
(62) Ditchfield, R.; Hehre, W. J.; Pople, J. A. *J. Chem. Phys.* **1971**, *54*, 724.
(63) Hehre, W. J.; Ditchfield, R.; Pople, J. A. *J. Chem. Phys.* **1972**, *56*, 2257.
(64) Ehlers, A. W.; Böhme, M.; Dapprich, S.; Gobbi, A.; Höllwarth, A.; Jonas, V.; Köhler, K. F.; Stegmann, R.; Veldkamp, A.; Frenking, G. *Chem. Phys. Lett.* **1993**, *208*, 111.
(65) Takano, Y.; Houk, K. N. *J. Chem. Theory Comput.* **2005**, *1*, 70.
(66) Toth, A. M.; Liptak, M. D.; Phillips, D. L.; Shields, G. C. *J. Chem. Phys.* **2001**, *114*, 4595.
(67) Fukui, K. *Acc. Chem. Res.* **1981**, *14*, 363.
(68) Gonzalez, C.; Schlegel, H. B. *J. Chem. Phys.* **1989**, *90*, 2154.
(69) Gonzalez, C.; Schlegel, H. B. *J. Phys. Chem.* **1990**, *94*, 5523.
(70) Frisch, M. J.; Trucks, G. W.; Schlegel, H. B.; Scuseria, G. E.; Robb, M. A.; Cheeseman, J. R.; Montgomery, J. A., Jr.; Vreven, T.; Kudin, K. N.; Burant, J. C.; Millam, J. M.; Iyengar, S. S.; Tomasi, J.; Barone, V.; Mennucci, B.; Cossi, M.; Scalmani, G.; Rega, N.; Petersson, G. A.; Nakatsuji, H.; Hada, M.; Ehara, M.; Toyota, K.; Fukuda, R.; Hasegawa, J.; Ishida, M.; Nakajima, T.; Honda, Y.; Kitao, O.; Nakai, H.; Klene, M.; Li, X.; Knox, J. E.; Hratchian, H. P.; Cross, J. B.; Bakken, V.; Adamo, C.; Jaramillo, J.; Gomperts, R.; Stratmann, R. E.; Yazyev, O.; Austin, A. J.; Cammi, R.; Pomelli, C.; Ochterski, J. W.; Ayala, P. Y.; Morokuma, K.; Voth, G. A.; Salvador, P.; Dannenberg, J. J.; Zakrzewski, V. G.; Dapprich, S.; Daniels, A. D.; Strain, M. C.; Farkas, O.; Malick, D. K.; Rabuck, A. D.; Raghavachari, K.; Foresman, J. B.; Ortiz, J. V.; Cui, Q.; Baboul, A. G.; Clifford, S.; Cioslowski, J.; Stefanov, B. B.; Liu, G.; Liashenko, A.; Piskorz, P.; Komaromi, I.; Martin, R. L.; Fox, D. J.; Keith, T.; Al-Laham, M. A.; Peng, C. Y.; Nanayakkara, A.; Challacombe, M.; Gill, P. M. W.; Johnson, B.; Chen, W.; Wong, M. W.; Gonzalez, C.; Pople, J. A. *Gaussian 03*, Revision D.1; Gaussian, Inc.: Waliingford, CT, 2005.
(71) Connors, K. A. In *Chemical Kinetics−The Study of Reaction Rate in Solution*; Wiley: New York, 1990; p 200.
(72) Alessio, E.; Balducci, G.; Lutman, A.; Mestroni, G.; Calligaris, M.; Attia, W. M. *Inorg. Chim. Acta*. **1993**, *203*, 205.
(73) Carpenter, J. E.; Weinhold, F. *J. Mol. Struct. (THEOCHEM)* **1988**, *169*, 41.
(74) Shi, Z.; Boyd, R. J. *J. Am. Chem. Soc*. **1989**, *111*, 1575.